Materials Research. 2019; 22(1): e20180458
DOI: http://dx.doi.org/10.1590/1980-5373-MR-2018-0458

Hydrogen Storage Properties and Reactive Mechanism of $LiBH_4/Mg_{10}YNi$-H Composite

Liu Yang[a], Shixin Zhao[a], Dongming Liu[a], Yongtao Li[a], Tingzhi Si[a]*

[a]*School of Materials Science and Engineering, Anhui University of Technology, Maanshan, Anhui 243002, P. R. China*

Received: July 02, 2018; Revised: October 20, 2018; Accepted: October 25, 2018

The $Mg_{10}YNi$ alloy was hydrogenated and then coupled with $LiBH_4$ to form $LiBH_4/Mg_{10}YNi$-H reactive hydride composite. The results indicate that thermal dehydrogenation stability of $LiBH_4$ can be remarkably reduced by combining with $Mg_{10}YNi$ hydride. The starting and ending temperatures for hydrogen desorption from the $LiBH_4/Mg_{10}YNi$-H composite are approximately 275 and 430 ºC, respectively. Dehydrogenation of the $LiBH_4/Mg_{10}YNi$-H composite proceeds mainly in two steps with a total reaction of $12LiBH_4 + 2.5Mg_{10}YNiH_{20} \rightarrow 24Mg + MgNi_{2.5}B_2 + 2.5YB_4 + 12LiH + 43H_2$. After rehydrogenation at 450 ºC under 9 MPa hydrogen pressure, the $LiBH_4/Mg_{10}YNi$-H composite starts to release hydrogen around 260 ºC, and as much as approximately 5.2 wt.% of hydrogen can be desorbed during the second dehydrogenation process.

Keywords: *Lithium borohydride, Reactive hydride composite, Hydrogen storage property, Reactive mechanism.*

1. Introduction

The increasing consumption of fossil fuels makes it urgent to develop new energy carriers, in which hydrogen shows great promise as an ideal alternative due to its high calorific value, clean burning products and abundant resources. For safely storing hydrogen with high efficiency, solid-state hydrogen storage materials have been intensively studied during the last several decades[1-6]. Among them, $LiBH_4$ has a theoretical hydrogen capacity as high as 13.8 wt.% through decomposition into LiH and B. However, the practical application of $LiBH_4$ is strongly limited by its high dehydrogenation temperature, sluggish dehydrogenation process and rigorous rehydrogenation conditions[7,8]. To overcome these deficiencies, various approaches such as catalyst addition[9-11], cation/anion substitution[12-14] and nano-confinement[15-17] have been developed and utilized.

Another effective way that has also been used to improve the hydrogen storage properties of $LiBH_4$ is the construction of reactive hydride composites[18-38]. The primary strategy of this method is to combine $LiBH_4$ with a reactive hydride destabilizer, thus reducing the overall dehydrogenation enthalpy and enhancing the rehydrogenation ability via the change in de-/hydrogenation pathway. The $LiBH_4/MgH_2$ (2:1) composite, as a typical example, was reported to release hydrogen with an enthalpy lowered by 25 kJ/mol H_2 with respect to the pristine $LiBH_4$ according to the altered reaction of $2LiBH_4 + MgH_2 \rightarrow MgB_2 + 2LiH + 4H_2$. In addition, the formation of MgB_2 upon dehydrogenation can make rehydrogenation easier to proceed by overcoming the chemical inertness of pure B[18]. Following this work, other binary metal hydrides (e.g., CaH_2[19], SrH_2[20], AlH_3[21], YH_3[22], CeH_2[23] and NdH_{2+x}[24]), single metal (e.g. Al[25] and Ni[26]), and complex hydrides (e.g. $LiAlH_4$[27], $NaAlH_4$[28], Li_3AlH_6[29], $Mg(AlH_4)_2$[30], $LiNH_2$[31] and $NaNH_2$[32]) were also used to combine with $LiBH_4$ to form reactive hydride composites.

Considering that better de-/hydrogenation properties of $LiBH_4$ might be obtained by simultaneously introducing two kinds of destabilizing components, the $LiBH_4$/Mg-X (X = Al, Fe, Ni or La) alloy hydride composites were developed and investigated[33-37]. For example, Zhou et al.[37] introduced the hydrogenated La_2Mg_{17} alloy into $LiBH_4$ by means of mechanochemical reaction under 40 bar hydrogen pressure and provided a synergetic thermodynamic and kinetic destabilization on the de/hydrogenation of $LiBH_4$ via the in situ formed MgH_2 and LaH_3. In our previous work[38], we prepared a reactive hydride composite of $LiBH_4/Mg_{11}CeNi$ hydride and improve the dehydrogenation property of $LiBH_4$ based on the combined destabilizing effect of Mg, Mg_2Ni and CeH_2. In order to enrich such an effect and further promote the development of $LiBH_4$-based hydrogen storage materials, the $LiBH_4/Mg_{10}YNi$-H composite was prepared to investigate its reversible hydrogen storage property and reactive mechanism in this paper.

2. Experimental Details

2.1 Sample preparation

Commercial $LiBH_4$ powder (95%, Alfa Aesar), Mg ribbon (90+%, Alfa Aesar), Ni foil (99.994%, Alfa Aesar) and Y ingot (99.9%, Alfa Aesar) were used as-received. The Mg_x YNi (x = 4, 10 and 12) alloys were prepared by induction melting of appropriate amounts of Mg, Y and Ni metals under argon atmosphere. In order to compensate the

*e-mail: ldm_ahut@163.com

losses of Mg and Y during melting, extra 18 wt.% of Mg and 3 wt.% of Y were added on the basis of stoichiometric amounts of starting materials, and the alloys were remelted two times to ensure homogeneity. After melting, the as-cast alloys were mechanically crushed into powders of 300 mesh and then subjected for hydrogen absorption/desorption. The $LiBH_4/Mg_{10}YNi$-H composite was prepared by ball-milling the mixture of $LiBH_4$ and $Mg_{10}YNi$ hydride with a 24:5 molar ratio under 0.5 MPa hydrogen pressure at a rotation speed of 400 rpm for 2 h using a QM-3SP2 planetary mill. Stainless steel vials (250 mL in volume) and balls (10 mm in diameter) were used. The ball to sample weight ratio was 30:1. To avoid air-exposure, all sample handling was carried out in an Ar-filled glove box equipped with a purification system, in which the typical O_2/H_2O levels are below 1 ppm.

2.2 Sample characterization

Hydrogen absorption/desorption properties of the samples were examined using a carefully calibrated Sieverts-type apparatus (Suzuki Shokan Co., Ltd., Japan). For the Mg-Y-Ni alloys, the powder samples were activated by two hydrogen absorption/desorption cycles. During each cycle, the samples were hydrogenated at 300 ºC under 4 MPa hydrogen pressure for 2 h and subsequently evacuated for 1 h. After activation, isothermal hydrogenation was performed at 300 ºC under the initial hydrogen pressure of 4 MPa. For the $LiBH_4/Mg_{10}YNi$-H composite, the temperature dependence of dehydrogenation was determined by heating the sample from ambient temperature to 500 ºC at the heating rate of 2 ºC/min under ~0.1 MPa hydrogen backpressure. Rehydrogenation of the samples was carried out at 450 ºC for 10 h under an initial hydrogen pressure of 6 or 9 MPa.

X-ray diffraction (XRD) measurements were performed using a Rigaku D/Max 2500VL/PC diffractometer with Cu Kα radiation at 50 kV and 150 mA. The XRD samples were loaded and sealed in a special holder that can keep the sample under argon atmosphere. In addition, the XRD pattern of the dehydrogenated product was analyzed with the Rietveld refinement program RIETAN-2000[39]. Fourier transform infrared (FTIR) spectra were collected at ambient conditions using a Nicolet 6700 FTIR spectrometer. The FTIR samples were prepared by cold pressing the mixture of testing powder and KBr with a 1:300 weight ratio.

3. Results and Discussion

3.1 Hydrogenation characteristics of Mg-Y-Ni alloys

Fig.1gives the isothermal hydrogenation curves of the Mg_xYNi (x = 4, 10 and 12) alloys after two hydrogen absorption/desorption cycles. It is observed that the hydrogenation reaction of the Mg_4YNi alloy is kinetically fast, with less than 40 min needed to complete the hydrogenation process. However, the saturated hydrogenation amount for the Mg_4YNi alloy is only approximately 3.4 wt.% because of a relative low Mg content. For the $Mg_{12}YNi$ alloy, though a higher hydrogenation amount can be obtained, the hydrogenation process cannot be finished within 160 min due to the inadequate catalytic effect of YH_2/YH_3 and Mg_2Ni (or Mg_2NiH_4) nanoparticles embedded in MgH_2 matrix[40,41]. In contrast, the $Mg_{10}YNi$ alloy can absorb as much as approximately 4.8 wt.% of hydrogen and accomplish the hydrogenation process within 100 min, exhibiting the best comprehensive property in terms of the hydrogenation amount and relative hydrogenation rate.

To clarify the hydrogenation mechanism, the XRD patterns of the $Mg_{10}YNi$ alloy as-cast and hydrogenated are shown in Fig. 2, indicating that the as-cast $Mg_{10}YNi$ alloy contains Mg, Mg_2Ni and MgY_2Ni_2, while the hydrogenated sample is composed of MgH_2, Mg_2NiH_4, YH_3 and little amount of YH_2. It can be superficially concluded that the $Mg_{10}YNi$ alloy reacted with H_2 to form MgH_2, Mg_2NiH_4, YH_3 and YH_2,

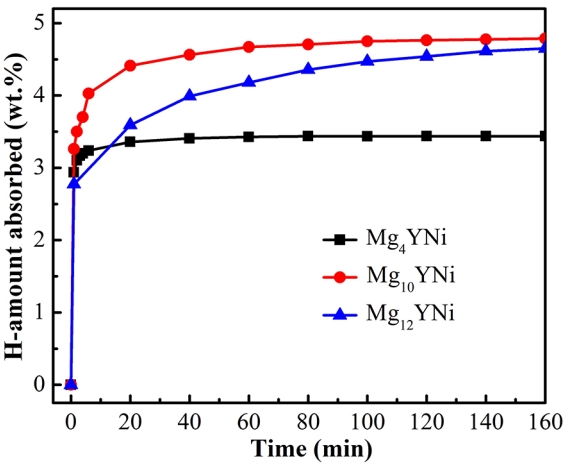

Figure 1. Isothermal hydrogenation curves of the Mg_xYNi (x = 4, 10 and 12) alloys after two hydrogen absorption/desorption cycles (the samples were hydrogenated at 300 °C under 4 MPa hydrogen pressure for 2 h and subsequently evacuated for 1 h).

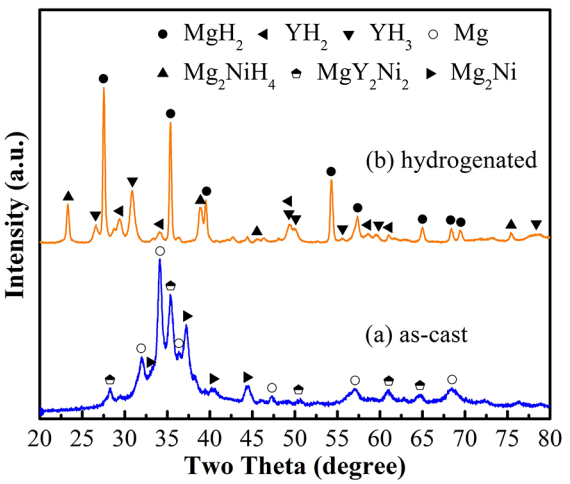

Figure 2. XRD patterns of the $Mg_{10}YNi$ alloy as-cast (a) and hydrogenated (b).

which is similar to other Mg-rich and Mg-RE-Ni alloys[40-43]. According to the hydrogenation amount of approximately 4.8 wt.% experimentally obtained, the hydrogen gas absorbed can be calculated to be 20 equivalents per $Mg_{10}YNi$.

3.2 Thermal dehydrogenation properties of $LiBH_4/Mg_{10}YNi$-H composite

The above hydrogenated $Mg_{10}YNi$ alloy was applied to couple with $LiBH_4$, and Fig. 3 gives the temperature-programmed dehydrogenation curve for the $LiBH_4/Mg_{10}YNi$-H composite. For comparison, the hydrogen desorption curve of pristine $LiBH_4$ is also included in Fig. 3. It can be seen that thermal dehydrogenation of the $LiBH_4/Mg_{10}YNi$-H composite starts around 275 ºC and proceeds mainly in two steps. The first step occurs in the temperature range from 275 to 350 ºC, and releases approximately 4.1 wt.% of hydrogen. The second step starts following the first one and finishes at approximately 430 ºC, with approximately 2.3 wt.% of hydrogen desorbed. In contrast, the pristine $LiBH_4$ starts to release detectable hydrogen at temperatures as high as 350 ºC, and only approximately 1.6 wt.% of hydrogen was desorbed when heating to 450 ºC. These results indicate that dehydrogenation stability of $LiBH_4$ can be remarkably reduced by combining with $Mg_{10}YNi$ hydride.

As reported in our previous work[30], thermal dehydrogenation of the $LiBH_4/MgH_2$ (2:1) composite initiates at approximately 340 ºC and cannot be accomplished even though the temperature rose to 550 ºC. For the $LiBH_4/YH_3$ (4:1) composite[44], as low as approximately 0.7 wt.% of hydrogen was desorbed at 350 ºC for 10 h under 0.1 MPa hydrogen backpressure. For the $LiBH_4/Mg_2NiH_4$ (4:5) composite[35], thermal dehydrogenation ends at approximately 450 ºC, with approximately 5.7 wt.% of hydrogen released. There can be no doubt that the present $LiBH_4/Mg_{10}YNi$-H composite exhibits lower dehydrogenation temperature and/or higher dehydrogenation amount than the individually MgH_2-, YH_3- or Mg_2NiH_4-coupled $LiBH_4$.

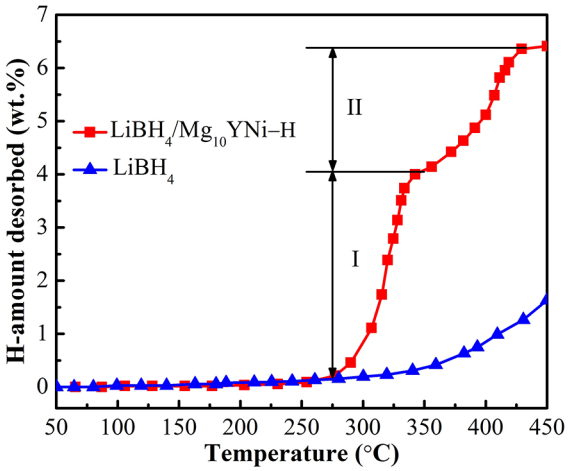

Figure 3. Temperature-programmed dehydrogenation curves of the $LiBH_4/Mg_{10}YNi$-H composite and pristine $LiBH_4$.

3.3 Dehydrogenation reactions of $LiBH_4/Mg_{10}YNi$-H composite

To elucidate the dehydrogenation reactive mechanism of the $LiBH_4/Mg_{10}YNi$-H composite, Figs. 4 and 5 present the XRD patterns and FTIR spectra of the samples after ball-milling and dehydrogenation at 350 and 450 ºC, respectively. As seen from Fig. 4a, the phases MgH_2, Mg_2NiH_4, YH_3 and YH_2 are present in the as-milled sample. Though $LiBH_4$ is not found in XRD data due to its relatively low content and/or amorphization by ball milling, the obvious signature bands for the B-H bond vibrations located at 2362, 2293, 2225 and 1126 cm^{-1} in Fig. 5a confirm its existence. The results suggest that no obvious reactions occurred between the starting materials during ball milling. When heating the $LiBH_4/Mg_{10}YNi$-H composite to 350 ºC, as shown in

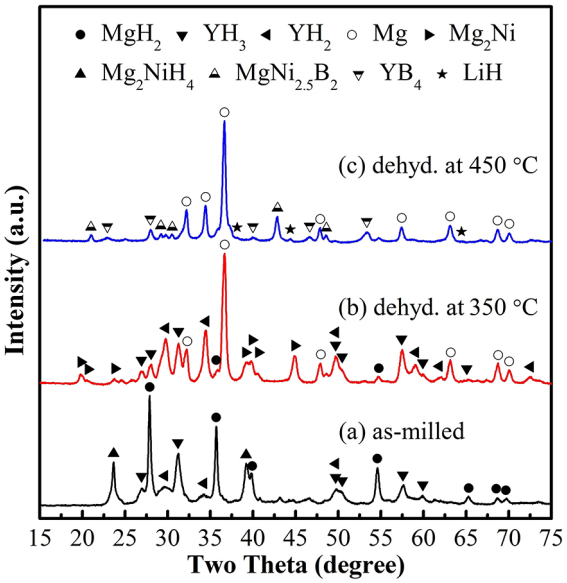

Figure 4. XRD patterns of the $LiBH_4/Mg_{10}YNi$-H composite as-milled (a) and dehydrogenated at 350 (b) and 450 °C (c), respectively.

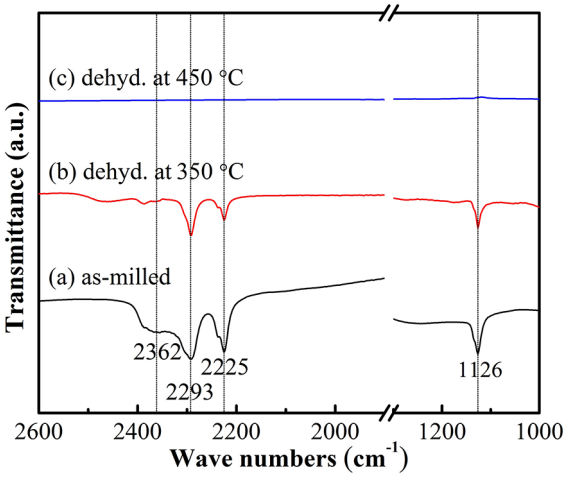

Figure 5. FTIR spectra of the $LiBH_4/Mg_{10}YNi$-H composite as-milled (a) and dehydrogenated at 350 (b) and 450 °C (c), respectively.

Figs. 4b and 5b, MgH_2 and Mg_2NiH_4 almost disappeared with the emergence of Mg and Mg_2Ni. In addition, the phase content of YH_2 is enhanced. Evidently, the first-step dehydrogenation for the $LiBH_4/Mg_{10}YNi$-H composite should be assigned to the decomposition of MgH_2 and Mg_2NiH_4 to form Mg and Mg_2Ni, respectively. Meanwhile, partial YH_3 decomposed into YH_2. Upon further increasing the dehydrogenation temperature to 450 ºC, the diffraction peaks arising form Mg_2Ni, YH_3 and YH_2 disappeared, and the solid residues are composed of Mg, $MgNi_{2.5}B_2$, YB_4 and LiH (see Fig. 4c). Moreover, almost no FTIR bands for the B-H bond vibrations can be observed in Fig. 5c, strongly implying that $LiBH_4$ was completely decomposed. To further confirm these existing phase components, the XRD pattern in Fig. 4c was refined by the Rietveld method. It can be seen from Fig. 6 that the diffraction pattern calculated from the structure models of the phases Mg, $MgNi_{2.5}B_2$, YB_4 and LiH is in good agreement with the measured pattern.

It is believed that the second-step dehydrogenation for the $LiBH_4/Mg_{10}YNi$-H composite should come from the decomposition of $LiBH_4$ that was reactively destabilized by Mg, Mg_2Ni, YH_3 and YH_2 together. The total dehydrogenation reaction can be expressed as:

$$12LiBH_4 + 2.5Mg_{10}YNiH_{20} \rightarrow 24Mg + MgNi_{2.5}B_2 + 2.5YB_4 + 12LiH + 43H_2 \quad (1)$$

According to this reaction, the $LiBH_4/Mg_{10}YNi$-H composite should theoretically release 6.7 wt.% of hydrogen. This estimated value is in good agreement with the measured value of 6.4 wt.% as indicated in Fig. 3. For the present case, Mg formed during the first-step dehydrogenation process can act as the heterogeneous nucleation center for the second-step dehydrogenation[37,38].

3.4 Rehydrogenation characteristics of $LiBH_4/Mg_{10}YNi$-H composite

For the purpose to evaluate the rehydrogenation property of the $LiBH_4/Mg_{10}YNi$-H composite, the dehydrogenated sample was subjected to rehydrogenation at 450 ºC under different hydrogen pressures (6 and 9 MPa, respectively), and then the second temperature-programmed dehydrogenation curves were measured. It is indicated from Fig. 7 that the rehydrogenation pressure has an important effect on the rehydrogenation and subsequent second dehydrogenation properties. For the sample rehydrogenated under 6 MPa hydrogen pressure, only approximately 4.2 wt.% of hydrogen was desorbed during the second dehydrogenation process, with an onset dehydrogenation temperature of approximately 290 ºC. In contrast, the sample rehydrogenated under 9 MPa hydrogen pressure starts to release hydrogen around 260 ºC, with as much as approximately 5.2 wt.% of hydrogen desorbed.

Figs. 8 and 9 give the XRD patterns and FTIR spectra of the rehydrogenated samples, respectively. As shown in Fig. 8a, MgH_2 and YH_3 were regenerated after rehydrogenation under 6 MPa hydrogen pressure. Increasing the rehydrogenation pressure to 9 MPa, as indicated in Fig. 8b, $LiBH_4$ and Mg_2NiH_4 were reformed with an enhancement of the relative contents of MgH_2 and YH_3. It can be seen from Fig. 9 that the FTIR bands for the B-H bond vibrations are present, demonstrating the regeneration of $LiBH_4$. In addition, the relatively higher intensity of FTIR bands in Fig. 9b than in Fig. 9a suggests a higher hydrogenation degree of the sample under 9 MPa hydrogen pressure. These results clearly show that reaction (1) can proceed reversibly under the present rehydrogenation conditions. Moreover, a higher rehydrogenation pressure is helpful to increase the hydrogen storage reversibility, which is consistent with the results obtained from Fig. 7.

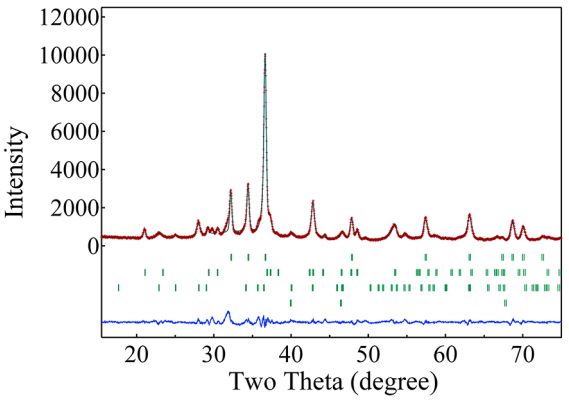

Figure 6. Rietveld refinement of the XRD pattern for the $LiBH_4/Mg_{10}YNi$-H composite dehydrogenated at 450 ºC. The vertical bars (from above) indicate the positions of Bragg diffraction for Mg, $MgNi_{2.5}B_2$, YB_4 and LiH, respectively. (The reliability factors for refinement are R_{wp} = 8.96%, R_p = 6.42% and S = 2.38)

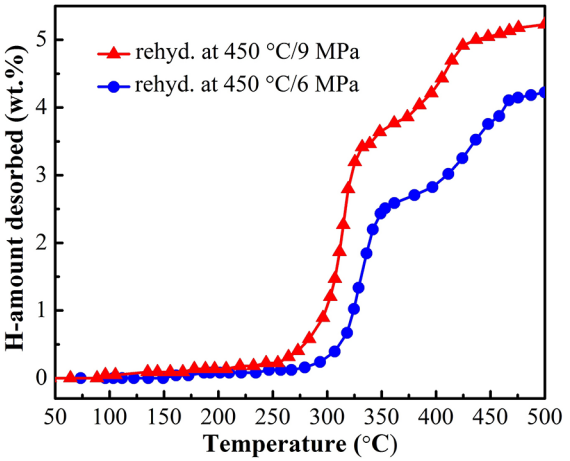

Figure 7. Second dehydrogenation curves of the $LiBH_4/Mg_{10}YNi$-H composite rehydrogenated at 450 ºC under 6 and 9 MPa hydrogen pressures, respectively.

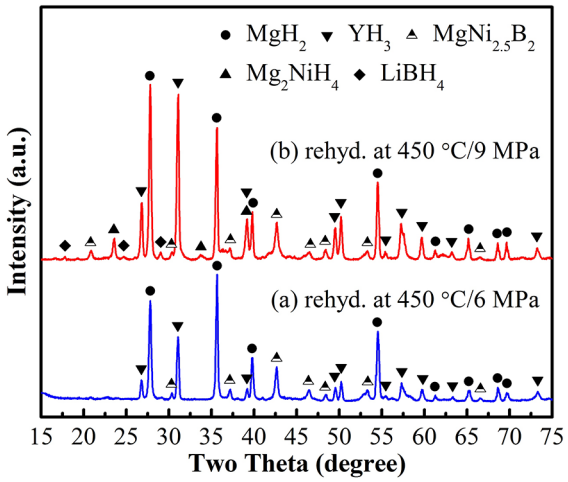

Figure 8. XRD patterns of the $LiBH_4/Mg_{10}YNi$-H composite after rehydrogenation.

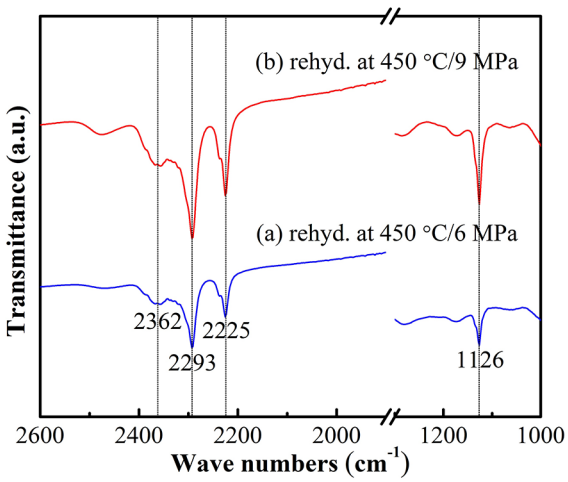

Figure 9. FTIR spectra of the $LiBH_4/Mg_{10}YNi$-H composite after rehydrogenation.

4. Conclusions

The hydrogen storage properties and reactive mechanism of the $LiBH_4/Mg_{10}YNi$-H composite were investigated. It was found that the $Mg_{10}YNi$ hydride shows a strong destabilization effect on $LiBH_4$, and that the $LiBH_4/Mg_{10}YNi$-H composite exhibits lower dehydrogenation temperature and/or higher dehydrogenation amount than the individually MgH_2-, YH_3- or Mg_2NiH_4-coupled $LiBH_4$. Dehydrogenation of the $LiBH_4/Mg_{10}YNi$-H composite proceeds mainly in two steps: one comes from the decomposition of MgH_2, Mg_2NiH_4 and partial YH_3, and the other can be assigned to the decomposition of $LiBH_4$ destabilized by Mg, Mg_2Ni, YH_3 and YH_2 together. After rehydrogenation at 450 ºC under 9 MPa hydrogen pressure, $LiBH_4$, MgH_2, Mg_2NiH_4 and YH_3 were regenerated, and as much as approximately 5.2 wt.% of hydrogen can be released during the second dehydrogenation process with an onset temperature of approximately 260 ºC.

5. Acknowledgments

This work was financially supported by the National Natural Science Foundation of China (Nos. U1503192 and 51371008) and the Key Project of Outstanding Young Talents in Universities of Anhui Province (No. gxyqZD2016067).

6. References

1. Schlapbach L, Züttel A. Hydrogen-storage materials for mobile applications. *Nature*. 2001;414:353-358.
2. Yang J, Sudik A, Wolverton C, Siegel DJ. High capacity hydrogen storage materials: attributes for automotive applications and techniques for materials discovery. *Chemical Society Reviews*. 2010;39(2):656-675.
3. Jena P. Materials for Hydrogen Storage: Past, Present, and Future. *The Journal of Physical Chemistry Letters*. 2011;2(4):206-211.
4. Lai Q, Paskevicius M, Sheppard DA, Buckley CE, Thornton AW, Hill MR, et al. Hydrogen Storage Materials for Mobile and Stationary Applications: Current State of the Art. *ChemSuschem*. 2015;8(17):2789-2825.
5. Rusman NAA, Dahari M. A review on the current progress of metal hydrides material for solid-state hydrogen storage applications. *International Journal of Hydrogen Energy*. 2016;41(28):12108-12126.
6. Yu X, Tang Z, Sun D, Ouyang L, Zhu M. Recent advances and remaining challenges of nanostructured materials for hydrogen storage applications. *Progress in Materials Science*. 2017;88:1-48.
7. Mauron P, Buchter F, Friedrichs O, Remhof A, Bielmann M, Zwicky CN, et al. Stability and Reversibility of $LiBH_4$. *The Journal of Physical Chemistry B*. 2008;112(3):906-910.
8. Züttel A, Rentsch S, Fischer P, Wenger P, Sudan P, Mauron P, et al. Hydrogen storage properties of $LiBH_4$. *Journal of Alloys and Compounds*. 2003;356-357:515-520.
9. Xu J, Qi Z, Cao J, Meng R, Gu X, Wang W, et al. Reversible hydrogen desorption from $LiBH_4$ catalyzed by graphene supported Pt nanoparticles. *Dalton Transactions*. 2013;42(36):12926-12933.
10. Wang J, Wang Z, Li Y, Ke D, Lin X, Han S, et al. Effect of nano-sized Ce_2S_3 on reversible hydrogen storage properties of $LiBH_4$. *International Journal of Hydrogen Energy*. 2016;41(30):13156-13162.
11. Huang X, Xiao X, Wang X, Yao Z, Wang C, Fan X, et al. Highly synergetic catalytic mechanism of Ni@g-C_3N_4 on the superior hydrogen storage performance of Li-Mg-B-H system. *Energy Storage Materials*. 2018;13:199-206.
12. Lindemann I, Borgschulte A, Callini E, Züttel A, Schultz L, Gutfleisch O. Insight into the decomposition pathway of the complex hydride $Al_3Li_4(BH_4)_{13}$. *International Journal of Hydrogen Energy*. 2013;38(6):2790-2795.

13. Olsen JK, Frommen C, Jensen TR, Riktor MD, Sørby MH, Hauback BC. Structure and thermal properties of composites with RE-borohydrides (RE = La, Ce, Pr, Nd, Sm, Eu, Gd, Tb, Er, Yb or Lu) and $LiBH_4$. *RSC Advances*. 2014;4:1570-1582.

14. Dovgaliuk I, Safin DA, Tumanov NA, Morelle F, Moulai A, Cerný R, et al. Solid aluminum borohydrides for prospective hydrogen storage. *ChemSuschem*. 2017;10(23):4725-4734.

15. Liu H, Jiao L, Zhao Y, Cao K, Liu Y, Wang Y, et al. Improved dehydrogenation performance of $LiBH_4$ by confinement into porous TiO_2 micro-tubes. *Journal of Materials Chemistry A*. 2014;2(24):9244-9250.

16. Thiangviriya S, Utke R. $LiBH_4$ nanoconfined in activated carbon nanofiber for reversible hydrogen storage. *International Journal of Hydrogen Energy*. 2015;40(11):4167-4174.

17. Guo L, Li Y, Ma Y, Liu Y, Peng D, Zhang L, et al. Enhanced hydrogen storage capacity and reversibility of $LiBH_4$ encapsulated in carbon nanocages. *International Journal of Hydrogen Energy*. 2017;42(4):2215-2222.

18. Vajo JJ, Skeith SL, Mertens F. Reversible Storage of Hydrogen in Destabilized $LiBH_4$. *The Journal of Physical Chemistry B*. 2005;109(9):3719-3722.

19. Li Y, Li P, Qu X. Investigation on $LiBH_4$-CaH_2 composite and its potential for thermal energy storage. *Scientific Reports*. 2017;7:41754.

20. Liu DM, Huang WJ, Si TZ, Zhang QA. Hydrogen storage properties of $LiBH_4$ destabilized by SrH_2. *Journal of Alloys and Compounds*. 2013;551:8-11.

21. Liu H, Wang X, Zhou H, Gao S, Ge H, Li S, et al. Improved hydrogen desorption properties of $LiBH_4$ by AlH_3 addition. *International Journal of Hydrogen Energy*. 2016;41(47):22118-22127.

22. Kim KB, Shim JH, Oh KH, Cho YW. Role of Early-Stage Atmosphere in the Dehydrogenation Reaction of the $LiBH_4$-YH_3 Composite. *The Journal of Physical Chemistry C*. 2013;117(16):8028-8031.

23. Mauron P, Bielmann M, Remhof A, Züttel A, Shim JH, Cho YW. Stability of the $LiBH_4$/CeH_2 Composite System Determined by Dynamic pcT Measurements. *The Journal of Physical Chemistry C*. 2010;114(39):16801-16805.

24. Cai W, Wang H, Sun D, Zhu M. Nanosize-Controlled Reversibility for a Destabilizing Reaction in the $LiBH_4$-NdH_{2+x} System. *The Journal of Physical Chemistry C*. 2013;117(19):9566-9572.

25. Hansen BRS, Ravnsbæk DB, Reed D, Book D, Gundlach C, Skibsted J, et al. Hydrogen Storage Capacity Loss in a $LiBH_4$-Al Composite. *The Journal of Physical Chemistry C*. 2013;117(15):7423-7432.

26. Xia GL, Guo YH, Wu Z, Yu XB. Enhanced hydrogen storage performance of $LiBH_4$-Ni composite. *Journal of Alloys and Compounds*. 2009;479(1-2):545-548.

27. Thaweelap N, Utke P. Dehydrogenation kinetics and reversibility of $LiAlH_4$-$LiBH_4$ doped with Ti-based additives and MWCNT. *Journal of Physics and Chemistry of Solids*. 2016;98:149-155.

28. Ravnsbaek DB, Jensen TR. Tuning hydrogen storage properties and reactivity: Investigation of the $LiBH_4$-$NaAlH_4$ system. *Journal of Physics and Chemistry of Solids*. 2010;71(8):1144-1149.

29. Wu X, Wang X, Cao G, Li S, Ge H, Chen L, et al. Hydrogen storage properties of $LiBH_4$-Li_3AlH_6 composites. *Journal of Alloys and Compounds*. 2012;517:127-131.

30. Liu D, Liu Q, Si T, Zhang Q, Fang F, Sun D, et al. Superior hydrogen storage properties of $LiBH_4$ catalyzed by $Mg(AlH_4)_2$. *Chemical Communications*. 2011;47(20):5741-5743.

31. Wolczyk A, Pinatel ER, Chierotti MR, Nervi C, Gobetto R, Baricco M. Solid-state NMR and thermodynamic investigations on $LiBH_4$-$LiNH_2$ system. *International Journal of Hydrogen Energy*. 2016;41(32):14475-14483.

32. Zhang Y, Tian Q. The reactions in $LiBH_4$-$NaNH_2$ hydrogen storage system. *International Journal of Hydrogen Energy*. 2011;36(16):9733-9742.

33. Han L, Xiao X, Fan X, Li Y, Li S, Ge H, et al. Enhanced dehydrogenation performances and mechanism of $LiBH_4$/$Mg_{17}Al_{12}$-hydride composite. *Transactions of Nonferrous Metals Society of China*. 2014;24(1):152-157.

34. Deng S, Xiao X, Han L, Li Y, Li S, Ge H, et al. Hydrogen storage performance of $5LiBH_4 + Mg_2FeH_6$ composite system. *International Journal of Hydrogen Energy*. 2012;37(8):6733-6740.

35. Vajo JJ, Li W, Liu P. Thermodynamic and kinetic destabilization in $LiBH_4$/Mg_2NiH_4: promise for borohydride-based hydrogen storage. *Chemical Communications*. 2010;46(36):6687-6689.

36. Sun T, Wang H, Zhang Q, Sun D, Yao X, Zhu M. Synergetic effects of hydrogenated Mg_3La and $TiCl_3$ on the dehydrogenation of $LiBH_4$. *Journal of Materials Chemistry*. 2011;21(25):9179-9184.

37. Zhou Y, Liu Y, Wu W, Zhang Y, Gao M, Pan H. Improved Hydrogen Storage Properties of $LiBH_4$ Destabilized by in Situ Formation of MgH_2 and LaH_3. *The Journal of Physical Chemistry C*. 2012;116(1):1588-1595.

38. Liu DM, Tan QJ, Gao C, Sun T, Li YT. Reversible hydrogen storage properties of $LiBH_4$ combined with hydrogenated $Mg_{11}CeNi$ alloy. *International Journal of Hydrogen Energy*. 2015;40(20):6600-6605.

39. Izumi F, Ikeda T. A Rietveld-Analysis Program RIETAN-98 and its Applications to Zeolites. *Materials Science Forum*. 2000;321-324:198-205.

40. Zhang QA, Liu DD, Wang QQ, Fang F, Sun DL, Ouyang LZ, et al. Superior hydrogen storage kinetics of $Mg_{12}YNi$ alloy with a long-period stacking ordered phase. *Scripta Materialia*. 2011;65(3):233-236.

41. Zhang QA, Zhang LX, Wang QQ. Crystallization behavior and hydrogen storage kinetics of amorphous $Mg_{11}Y_2Ni_2$ alloy. *Journal of Alloys and Compounds*. 2013;551:376-381.

42. Zhang QA, Jiang CJ, Liu DD. Comparative investigations on the hydrogenation characteristics and hydrogen storage kinetics of melt-spun $Mg_{10}NiR$ (R = La, Nd and Sm) alloys. *International Journal of Hydrogen Energy.* 2012;37(14):10709-10714.

43. Fan Y, Peng X, Su T, Bala H, Liu B. Modifying microstructures and hydrogen storage properties of 85 mass% Mg-10 mass% Ni-5 mass% La alloy by ultra-high pressure. *Journal of Alloys and Compounds*. 2014;596:113-117.

44. Kim KB, Shim JH, Cho YW, Oh KH. Pressure-enhanced dehydrogenation reaction of the $LiBH_4$-YH_3 composite. *Chemical Communications*. 2011;47(35):9831-9833.